Adsorption Phenomena of Cubane-Type Tetranuclear Ni(II) Complexes with Neutral, Thioether-Functionalized Ligands on Au(111)

Volkmar Heß [a], Frank Matthes [a], Daniel E. Bürgler [a,*], Kirill Yu. Monakhov [b,*], Claire Besson [b], Paul Kögerler [b], Alessio Ghisolfi [c], Pierre Braunstein [c], and Claus M. Schneider [a]

[a] *Peter Grünberg Institute, Electronic Properties (PGI-6) and Jülich-Aachen Research Alliance, Fundamentals for Future Information Technology (JARA-FIT), Forschungszentrum Jülich, 52425 Jülich, Germany.*

[*] *E-mail: d.buergler@fz-juelich.de*

[b] *Institut für Anorganische Chemie and Jülich-Aachen Research Alliance, Fundamentals for Future Information Technology (JARA-FIT), RWTH Aachen University, Landoltweg 1, 52074 Aachen, Germany.*

[*] *E-mail: kirill.monakhov@ac.rwth-aachen.de*

[c] *Laboratoire de Chimie de Coordination, Institut de Chimie (UMR 7177 CNRS), Université de Strasbourg, 4 rue Blaise Pascal, 67081 Strasbourg, France.*

Keywords: Single-Molecule Studies; Thioethers; Molecular Magnets; Photoelectron Spectroscopy; Scanning Tunneling Microscopy

Abstract

The controlled and intact deposition of molecules with specific properties onto surfaces is an emergent field impacting a wide range of applications including catalysis, molecular electronics, and quantum information processing. One strategy is to introduce grafting groups functionalized to anchor to a specific surface. While thiols and disulfides have proven to be quite effective in combination with gold surfaces, other S-containing groups have received much less attention. Here, we investigate the surface anchoring and organizing capabilities of novel charge-neutral heterocyclic thioether groups as ligands of polynuclear nickel(II) complexes. We report on the deposition of a cubane-type $\{Ni_4\}$ (= $[Ni(\mu_3\text{-}Cl)Cl(HL{\cdot}S)]_4$) single-molecule magnet from dichloromethane solution on a Au(111) surface, investigated by scanning tunneling microscopy, X-ray photoelectron spectroscopy, and low-energy

electron diffraction, both immediately after deposition and after subsequent post-annealing. The results provide strong evidence for partial decomposition of the coordination complex upon deposition on the Au(111) surface that, however, leaves the magnetic $\{Ni_4Cl_{4n}\}$ (n = 1 or 2) core intact. Only post-annealing above 480 K induces further decomposition and fragmentation of the $\{Ni_4Cl_{4n}\}$ core. The detailed insight into the chemisorption-induced decomposition pathway not only provides guidelines for the deposition of thioether-functionalized Ni(II) complexes on metallic surfaces but also reveals opportunities to use multidentate organic ligands decorated with thioether groups as transporters for highly unstable inorganic structures onto conducting surfaces, where they are stabilized retaining appealing electronic and magnetic properties.

1. Introduction

The prospects of using molecules with prominent properties for material chemistry and surface physics as well as nanoelectronic, nanospintronic, or catalytic applications are motivated by their dimensions, relative ease of synthesis and tunability, and structural, electronic and magnetic versatility. One of the most important challenges for a wide range of applications including supported-metal complex catalysis, molecular electronics and spintronics, and quantum information processing is the controlled deposition of molecules on conducting surfaces and the understanding of the associated physisorption and chemisorption phenomena, which may inhibit the desired molecular properties.

This objective has led to the use of grafting groups to better control the molecule-surface interaction. With respect to stable and controlled anchoring, the formation of self-assembled monolayers (SAM) of sulfur-functionalized molecules on gold surfaces has proven a scalable method, in particular for molecules with thiol end-groups [1-4]. However it is *a priori* unknown if and how a specific grafting group and its binding to the substrate is going to affect the molecular properties after adsorption. For example, $\{Mn_{12}\}$ molecules with thiol-based grafting groups deposited on gold lose the characteristic features of a single-molecule magnet (SMM) [5], whereas $\{Fe_4\}$ SMMs on gold retain their magnetic properties owing to the decoupling of the magnetic core from the surface by suitable, bulky spacer groups [6,7]. While thiols (–

SH) [8], methyl sulfides (–SMe) [9], and 1,2-dithiolanes (–S-S–) [10] have proven to be effective anchoring groups to gold electrodes in the chemistry and physics of magnetic coordination complexes [11], other thioether-like groups such as cyclic thioethers are still unexplored. The systematic investigation of the adsorption phenomena of metal-organic molecules on various metallic surfaces and thus of the generated molecule-substrate hybrids is appealing and worthwhile because it should allow to derive necessary guidelines for the fine-tuning of the critical metal-ligand coordination bonds and the structure and composition of the molecular material.

Here, we report our efforts to expand the strategy of using thiols as aurophilic deposition groups, for the first time, to aliphatic cyclic, *i.e.* semi-rigid, thioether functions. This strategy aims at taking advantage of the facts that thioether grafting groups are less prone to oxidation and are also suitable for the production of SAMs on coinage metal surfaces [12-14] by forming a weaker coordination-type bond. We present the adsorption characteristics and thermal stability of a thio-cyclohexane-functionalized $\{Ni_4\}$ cubane-type complex, recently identified in bulk samples as an SMM [15], on Au(111) using combined X-ray photoelectron spectroscopy (XPS), scanning tunneling microscopy (STM), and low-energy electron diffraction (LEED). Our study represents an important first step towards the design of a material of electronic and magnetic, but also catalytic (*e.g.* heterogeneous catalysis with Ni(II) centers [16]) relevance.

2. Molecule properties

Recently, we reported the synthesis, structure, and magnetochemistry of the cubane-type nickel(II) complex $\{Ni_4\}$ with the formula $[Ni(\mu_3\text{-}Cl)Cl(HL{\cdot}S)]_4$ containing four neutral pyridyl-alcohol-type ligands ($HL{\cdot}S = C_{11}H_{15}NOS$) with structurally exposed, peripheral thio-cyclohexane functionalities (Fig. 1) [15]. The four octahedrally coordinated nickel centers form a distorted $\{Ni_4(\mu_3\text{-}Cl)_4\}$ cubane core, the remaining three coordination sites per nickel center are occupied by a terminal chloride ligand and the N and O donor sites of one chelating HL·S ligand. In contrast to the previously investigated cubane-type $[Co^{II}_4Cl_4(HL)_4]$ SMMs (ratio Co/HL/Cl = 1:1:1) [17], the present system $\{Ni^{II}(\mu_3\text{-}Cl)Cl\}_4{\leftarrow}(HL{\cdot}S)_4$ (ratio Ni/HL·S/Cl = 1:1:2) does not involve charge

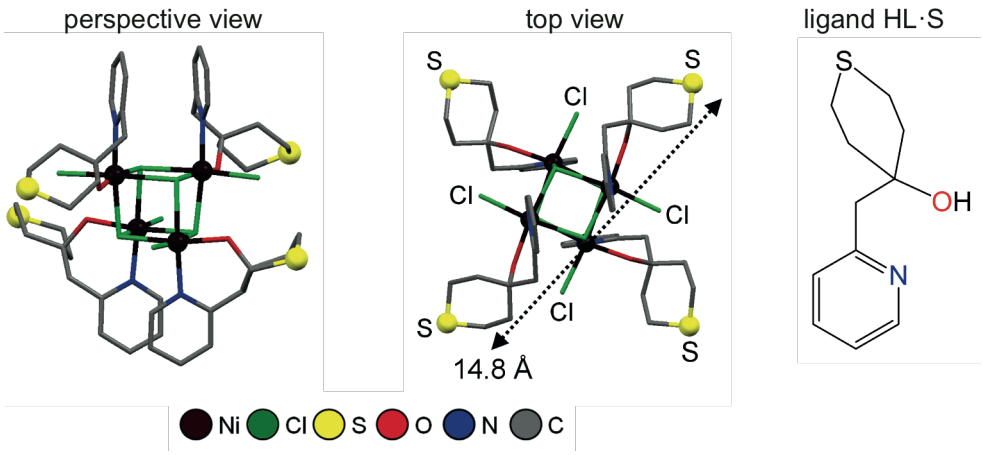

Fig. 1. Perspective (left) and top (middle) views of the molecular structure of $[Ni(\mu_3\text{-}Cl)Cl(HL{\cdot}S)]_4$, where HL·S represents a pyridyl-alcohol-type ligand with an aliphatic cyclic thioether group (right). The nickel and sulfur atoms are represented as ball-and-stick models. Hydrogen atoms are omitted for clarity.

transfer between the magnetic core metals and the HL·S ligands. This allows us to address the effect of the ligand's charge neutrality on the adsorption characteristics of our cubane-type tetranuclear Ni(II) complex.

As a polycrystalline material, $\{Ni_4\}$ is stable up to about 525 K under protective atmosphere and soluble in dichloromethane (DCM). The stability in DCM solution was proven by FT-IR spectroscopy [15]. The $\{Ni_4\}$ SMM has a diameter of about 15 Å (S to S) and its magnetism is characterized by ferromagnetic coupling between the Ni ions ($J = +10.6$ cm^{-1}) and a blocking temperature of 3.8 K [15].

2. Experimental

2.1 Instrumental

STM, LEED, and most of the XPS measurements (see below) were performed in a multi-chamber UHV comprising a loadlock, a preparation chamber, and an analysis chamber. The preparation chamber with a base pressure of $1 \cdot 10^{-10}$ mbar is equipped with sputtering and annealing devices and also features sample characterization tools like Auger electron spectroscopy (AES), XPS, and LEED. The analysis chamber reaches a base pressure of $5 \cdot 10^{-11}$ mbar and is equipped with a low-temperature STM from Omicron. We used homemade etched tungsten STM-tips, which were flashed *in-situ* to remove

oxide layers. The gap voltage is applied to the tip and the sample is grounded. The STM scanner was calibrated with Si(111)-7x7 samples.

The spectra in Figs. 3 and 4 were taken *in-situ* using a lab-based Mg Kα radiation source and a hemispherical analyzer from Omicron operated with an energy resolution of 1 eV. XPS spectra in Figs. 2a-d were taken at beamline 5 of the DELTA synchrotron in Dortmund. The energy resolution was about 0.1 eV. The spectrum in Fig. 2e was measured in a stand-alone XPS machine with monochromatized Al Kα radiation (PHI 5000 VersaProbe II) yielding an overall energy resolution of 0.4 eV. All XPS measurements were performed at room temperature. For a meaningful comparison, all spectra were normalized to the Au $4f_{7/2}$ peak at 84.0 eV and the elemental composition was calculated by applying the sensitivity factors taken from Ref. [18].

The heater in the multi-chamber UHV system was calibrated using a type-K thermocouple attached to the front side of the Au(111) sample holder used in this experiment. The temperature on top of the Au(111) substrate might be slightly lower. The heater available at beamline 5 at DELTA allowed temperature control with an accuracy of about ±25 K.

2.2 Sample preparation

The preparation of the Au(111) substrates and the measurements on the chemisorbed films were performed under ultra-high vacuum (UHV) conditions, whereas the molecule deposition out of DCM was performed under protective argon atmosphere during a vacuum break of about two hours that also includes exposure to ambient atmosphere.

The Au(111) single crystal substrate was cleaned *in-situ* by sputtering for 30 min with 800 eV Ar ions at $5 \cdot 10^{-6}$ Acm^{-2} current density and $5 \cdot 10^{-6}$ mbar Ar partial pressure. Subsequently, the crystal was heated to 900 K by a tungsten filament and slowly cooled down to room temperature to heal the sputter-induced defects and restore the intrinsic herringbone reconstruction [19] of this surface. Afterwards XPS and AES revealed no contamination, and a clean surface was also confirmed by the observation of the herringbone reconstruction in STM (Fig. 5a).

{Ni_4} thin films in the monolayer (ML) regime were deposited *ex-situ* by immersing the previously cleaned Au(111) crystal surface into an oxygen-free 0.5 mM {Ni_4}-DCM solution for one hour. Afterwards the crystal was immersed into pure DCM again for one hour to remove unbound species and contaminations. The deposition was conducted under argon atmosphere and at room temperature.

The {Ni_4} bulk sample for XPS reference measurements was prepared by drop casting about 20 µl oxygen-free 0.5 mM {Ni_4}-DCM solution on a clean Au(111) crystal without applying subsequent rinsing in pure DCM.

3. Results and discussion

After deposition the samples were immediately transferred back into the UHV system, where the organic films are first investigated in the as-deposited state and subsequently after *in-situ* post-annealing to several temperatures.

3.1 XPS results

We used XPS as a very sensitive tool to investigate the binding mode of the {Ni_4} complex to the Au(111) surface by studying the peak fine structure of the S 2p signal and the binding energy of the Ni 2p doublet.

3.1.1 As-deposited state

Since the binding of the {Ni_4} to the surface is expected to be solely accomplished via the S-containing ligands, we first investigated the surface binding capabilities of the bare HL·S ligand without the central {$Ni_4(\mu_3\text{-}Cl)_4Cl_4$} cube as a reference. The results are shown in Fig. 2a and reveal that the S 2p signal consists of four components resulting from the superposition of three doublets with the $2p_{3/2}$ peak located at 161.1, 162.1, and 163.1 eV, respectively. The relative weights of the doublets are listed in Table 1 and agree well with previous literature reports on thioether-functionalized molecules [20]. The doublet at 163.1 eV, which is responsible for 52.9% of the total signal, is attributed [20] to a weak coordination-type bond, which is the expected binding for a thioether group. The doublets at 162.1 and 161.1 eV have basically the same intensity and are responsible for the remaining 47.1% of the signal. The

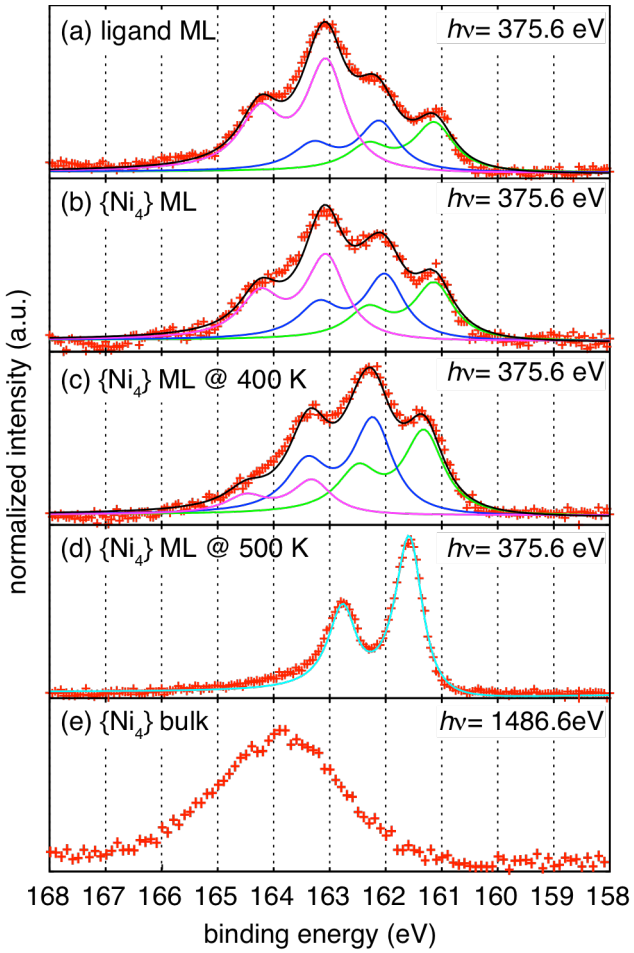

Fig. 2. Normalized XPS S 2p spectra after deposition of (a) bare HL·S ligands on Au(111), and (b-d) $\{Ni_4\}$ complexes on Au(111), and (e) the $\{Ni_4\}$ bulk reference sample. Post-annealing temperatures for (c) and (d) are indicated. Red crosses represent experimental data and solid lines in (a-d) the decomposition of the spectra into individual doublets at 161.1 eV (green), 161.6 eV (cyan), 162.1 eV (blue), and 163.1 eV (pink) according to Table 1. Black lines are the fitted total spectra. The background was subtracted with a Shirley algorithm. All S 2p doublets were fitted with a fixed $2p_{3/2}$:$2p_{1/2}$ intensity ratio of 2 and a fixed energy splitting of 1.19 eV by Doniach-Sunjic functions with an asymmetry of –0.1 and a peak width of 0.32 eV. Experiments are carried out for (a-d) at BL 5 at DELTA with a photon energy of 375.6 eV and for (e) with a stand-alone spectrometer using monochromatized Al Kα radiation.

doublet at 162.1 eV is usually attributed [20,21] to a thiol group bound to gold. The 161.1 eV peak is either due to atomic sulfur or due to a thiol group with different binding chemistry [20,22], *e.g.* different binding site on the reconstructed Au(111) surface. For thioethers, both destructive [23] and non-destructive [24] adsorption on gold have been reported. Nevertheless, the appearance in our case of ca. 50% thiols is surprising and inscrutable, but in

Table 1. Relative intensities of the S 2p doublets in the XPS spectra in percent. Doublets are named by the energy position of the $2p_{3/2}$ peak.

S $2p_{3/2}$ peak energy (eV)	163.1	162.1	161.6	161.1
Species	Thioether	Thiol 1	Atomic S	Thiol 2
HL·S Ligand	52.9	23.9	0	23.4
$\{Ni_4\}$	41	31.8	0	27.2
$\{Ni_4\}$ @ 400 K	16	44.7	0	39.3
$\{Ni_4\}$ @ 500 K	0	0	100	0

agreement with Ref. [20]. The XPS reference measurement of a bulk $\{Ni_4\}$ sample (Fig. 2e) reveals a strongly broadened S 2p peak with maximum intensity at 163.9 eV that we consider to be a fingerprint of the HL·S ligands when not bound to the Au substrate. From the absence of this component in Fig. 2a, we conclude that all unbound species are removed from the ligand reference sample by our deposition procedure, as expected.

Next we deposited the $\{Ni_4\}$ complex and confirmed the presence of all elements (except H) on the surface that constitute $\{Ni_4\}$ by XPS (Fig. S1 in the Supplementary Material). The S 2p spectrum (Fig. 2b) is quite similar to that of the adsorbed bare ligands (Fig. 2a). The S 2p signal consists of the same three doublets with slightly different weights (Table 1). For the intact $\{Ni_4\}$ it is geometrically impossible that all four ligands are bound to the gold substrate at the same time. Assuming all ligands remain attached to $\{Ni_4\}$ we would expect that only one or two ligands per complex bind to Au, resulting in the XPS spectra in a component of the unbound species (Fig. 2e) with a weight of 50-75%. The fact that we do not observe such a component at all indicates that $\{Ni_4\}$ loses at least some of its ligands during deposition. The question whether all ligands are detached cannot be answered by XPS, but will be addressed later by STM. In both cases of bare ligand and complete $\{Ni_4\}$ deposition, a broadened C 1s peak was detected at 284.5 eV, which is a typical value for C in organic ligands [20].

3.1.2 Post-annealed states

To gain more insight into the thermal stability and surface binding conditions, we post-annealed the samples under UHV conditions. After 30 min

at 400 K, we observed a change of the S 2p weights (Fig. 2c and Table 1). The amount of intact thioethers was reduced, while the contributions from the thiols were increased. By increasing the thermal energy, more ligands seem to transform into an energetic more favorable thiol form. After 30 min post-annealing at 500 K, we observed only one doublet at 161.6 eV (Fig. 2d and Table 1), and heating to higher temperatures did not change the S spectrum anymore. The evolution of all three former doublets into a new one indicates significant changes of the S-containing ligand, most likely decomposition by releasing atomic S that binds to the gold surface.

Additional evidence for a ligand decoordination upon interaction with the surface stems from the electrochemical analysis of a gold electrode that is functionalized by the same treatment applied to the Au crystal for the *in-situ* measurements: It shows the same correlated oxidation and reduction waves as those appearing after a first non-reversible oxidation in $\{Ni_4\}$ using a glassy carbon electrode (Fig. S2 in the Supplementary Material). This indicates that the species deposited on gold is distinct from the intact $\{Ni_4\}$ complex and that the ligand decoordination process observed upon absorption is most likely initiated by electron transfer from the molecule to the metallic substrate.

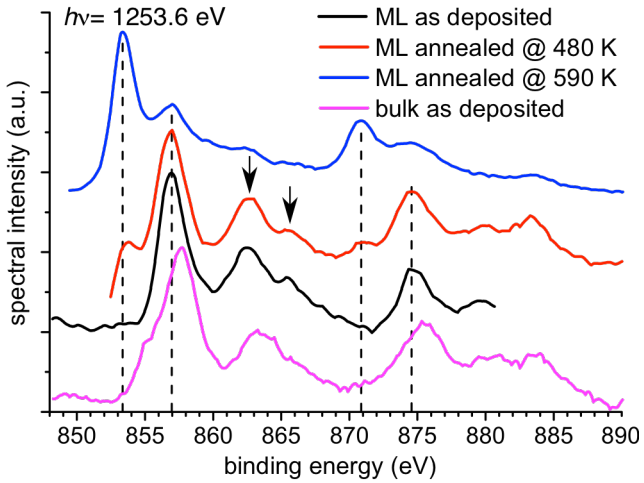

Fig. 3. Shift of the Ni 2p doublet upon post-annealing. Before annealing (black) the Ni $2p_{3/2}$ peak is at 857 eV in good agreement with Ni(II) in a Cl environment. After subsequent annealing steps at 590 K, the Ni $2p_{3/2}$ peak shifts to 853.5 eV (blue) indicating the decomposition of the central cubane-like $\{Ni_4Cl_{4n}\}$ core. The Ni $2p_{1/2}$ peak shows an analogue behavior. The pink spectrum of a $\{Ni_4\}$ bulk sample is slightly shifted with respect to the as deposited monolayer sample, but shows a very similar overall spectral shape. Black arrows mark the shake-up satellites.

Another interesting question concerns the state of the remaining $\{Ni_4Cl_{4n}\}$ (n = 1 or 2) core. For $n = 2$ the $\{Ni_4Cl_4\}$ core is decorated by four terminal Cl atoms (Fig. 1), and $n = 1$ corresponds to the naked core. In a $\{Ni_4\}$ bulk reference sample, we detect the Ni $2p_{3/2}$ peak at 857.7 eV (pink line in Fig. 3). The presence of O and N donors in $\{Ni_4\}$ possibly explains the shift in binding energy of 0.7 eV with respect to $NiCl_2$ [25]. In addition, we observe the two typical shake-up satellites (black arrows in Fig. 3) for a $NiCl_2$ film [26], in which the Ni is also octahedrally coordinated. The Ni 2p XPS spectrum of a $\{Ni_4\}$ monolayer sample in the as-deposited state (black line in Fig. 3) shows a very similar overall spectral shape, including the shake-up satellites, to the bulk sample, but the spectrum is shifted by 0.7 eV to lower binding energy. The similarity indicates that the cubane-like $\{Ni_4Cl_{4n}\}$ core is still intact after deposition although the ligands are decoordinated, which most likely gives rise to the slight shift in binding energy. In this context, it is also worthwhile to note that the detachment of the neutral ligands does not alter the charge on the remaining fragment, making it likely to be the cubane-like $\{Ni_4Cl_{4n}\}$ core of the parent molecule. The appearance of the shake-up satellites in the black and red spectra in Fig. 3 suggests paramagnetic behavior [26] of the core at room temperature, *i.e.* the measurement temperature. The Cl $2p_{3/2}$ peak is detected at 199 eV (Fig. S1 in the Supplementary Material), which is in good agreement with the expected Ni environment [25] and again confirms the integrity of the cubane-like $\{Ni_4Cl_{4n}\}$ core after deposition. However, from the XPS data we cannot state whether the terminal Cl atoms are still attached. If they were decoordinated but bound to the surface, they would still contribute to the spectra.

Upon post-annealing to 590 K, we observe a significant shift of the Ni $2p_{3/2}$ peak by 3.5 eV (blue spectrum in Fig. 3). The total disappearance of Cl in the XPS spectra at this temperature (Fig. 4) provides strong evidence for the breaking of the central cubane-like $\{Ni_4Cl_{4n}\}$ core during annealing. After annealing, the Ni 2p binding energy is closer to that of bulk Ni^0, implying at least a change in chemical environment but more likely a change in oxidation state from initially +II to 0.

Magnetic studies of the intact cubane-like $\{Ni_4Cl_{4n}\}$ core remaining on the surface after the detachment of the charge-neutral HL·S organic ligands are

beyond the scope of this study and will be reported elsewhere. To this end our next studies will include the investigation of the magnetic properties of the cubane-like $\{Ni_4Cl_{4n}\}$ core on the surface by X-ray magnetic circular dichroism (XMCD) alongside computational studies of this material on the nanoscale. Additionally, we are currently examining the magnetic properties of the bulk $\{Ni_4\}$ coordination cluster in the low-temperature regime at low magnetic fields.

3.1.3 Decomposition upon *in-situ* post-annealing

All changes of the elemental composition induced by stepwise post-annealing were monitored by lab-based XPS (Fig. 4). For low temperatures we observe no significant change in the elemental composition. Starting at 480 K, the O and N signal intensities strongly decrease indicating that the thermal stability of $\{Ni_4\}$ is reduced when deposited on a surface as compared to the stability in bulk (525 K) evidenced by thermogravimetric analysis (TGA) [15]. At 590 K the intensity of Cl drops significantly, and at 680 K neither O, N, nor Cl can be detected anymore, which clearly establishes the decomposition of the molecule in agreement with all previous statements. The amount of S is constant within the error bars of the XPS analysis, indicating that all S atoms are indeed bound to the Au substrate. This observation further supports the conjecture of ligand detachment during adsorption.

When discussing mechanisms for the observed molecular decomposition it is useful to consider relevant energy scales. The thermal energy involved in the post-annealing process ($kT \approx 25$ - 70 meV) is small in comparison to the adsorption energies of S on Au, which have been calculated using density functional theory (DFT) to be as high as 4 eV for single S atoms, depending on adsorption geometry [27]. For thiols, DFT calculations lead to adsorption energies of 1-2 eV, depending on adsorption geometry [27]. For the related thiophene molecule, adsorption energies on Cu(100) of 630 meV have been reported [28]. Thus, it seems safe to assume that the adsorption energy of the thioether-functionalized $\{Ni_4\}$ is at least one order of magnitude larger than the thermal energies involved in the post-annealing process. Therefore, it is very likely that the adsorption energy is the driving force behind the decomposition of the $\{Ni_4\}$ complex. However, higher adsorption energies do not necessarily

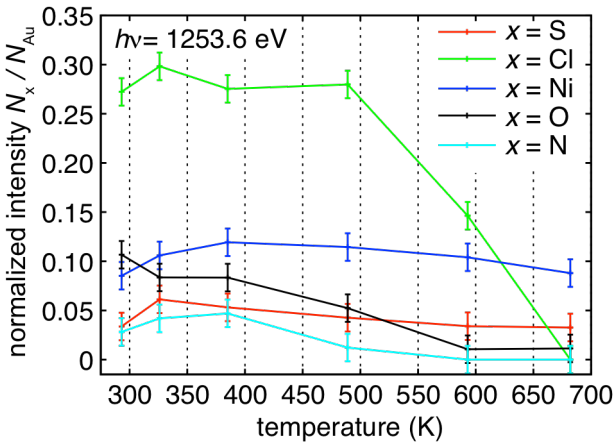

Fig. 4. Elemental composition as a function of the post-annealing temperature reached in subsequent annealing steps. At higher annealing temperatures, the signals for O, N, and Cl completely vanish due to the decomposition of the $\{Ni_4\}$ complex. The S and Ni signals, however, are within the error bar constant during the whole annealing procedure.

cause more frequent molecular decomposition, but may result in increased molecular stability after adsorption, as recently reported [29]. Since there are only a few reports on the deposition of bulky thioether-functionalized molecules on gold [30], it is difficult to answer this question at the current stage. Nevertheless, our data suggest a separation of the ligands from the core directly when the cubane cluster is deposited on the surface. The post-annealing treatment then leads first to the decomposition of the ligands and, at higher temperatures, to the disintegration of the central cubane-like $\{Ni_4Cl_{4n}\}$ core.

3.2 STM results

3.2.1 As-deposited state

Fig. 5a shows a typical STM image of the herringbone reconstruction of the clean Au(111) surface, and Fig. 5b the surface morphology after the $\{Ni_4\}$ deposition process, where no herringbone reconstruction is visible anymore. Instead the terraces appear to be covered by a diffuse “blanket” and irregularly shaped particles. The main focus of the STM study was to potentially image intact $\{Ni_4\}$ complexes or fragments, such as the ligand or the $\{Ni_4Cl_{4n}\}$ core. In literature the formation of highly ordered SAMs with thioether-functionalized molecules has been reported [12,13], but in our case no signs of any ordered structures or monoatomic depressions typically for highly ordered

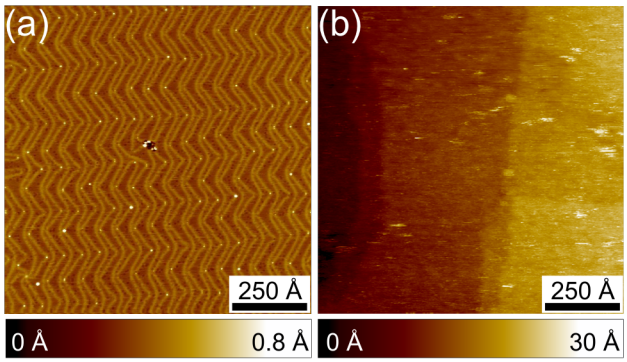

Fig. 5. Surface morphology before and after $\{Ni_4\}$ deposition. (a) STM image of the cleaned Au(111) substrate showing up to 1000 Å wide terraces with a regular herringbone reconstruction. Image parameters: 1000 Å x 1000 Å, $V_{Bias} = -1$ V, $I_T = 1$ nA, 78 K. (b) STM image after $\{Ni_4\}$ deposition on the surface shown in (a) without post-annealing. Image parameters: 1000 Å x 1000 Å, $V_{Bias} = -1$ V, $I_T = 50$ pA, 5 K.

SAMs [31] could be observed. Larger molecules, such as most SMMs with multiple potential adsorption positions, usually show disordered adsorption patterns [6,7]. These molecules can then be identified by statistically analyzing the particle size. Although we observe irregularly shaped particles, they show a random lateral size distribution and are typically much larger than a single $\{Ni_4\}$ cubane or its fragments. Zooming in these particles did not reveal any additional details. Thus, it seems very unlikely that these represent single $\{Ni_4\}$ or well-defined clusters of $\{Ni_4\}$.

Also LEED of the as-deposited state only shows weak Au(111)-(1x1) spots indicating no additional order. Therefore, we believe that the fragments resulting from the decomposition of $\{Ni_4\}$ are lying in a disordered fashion on the surface and give rise to the diffuse STM morphology.

3.2.2 Post-annealing at 590 K

Fig. 6a shows a STM picture after annealing at 590 K for one hour, resulting in a completely different morphology with ordered, disordered, and also uncovered areas. In a few spots, we also observe some larger features, which might be identical to those in the images taken prior to the post-annealing (Fig. 5b). The uncovered areas reveal a distorted herringbone reconstruction of the bare Au(111) surface (inset of Fig. 6a). Changes in the electronic structure due to the adsorption of particles can lead to a distortion of the herringbone

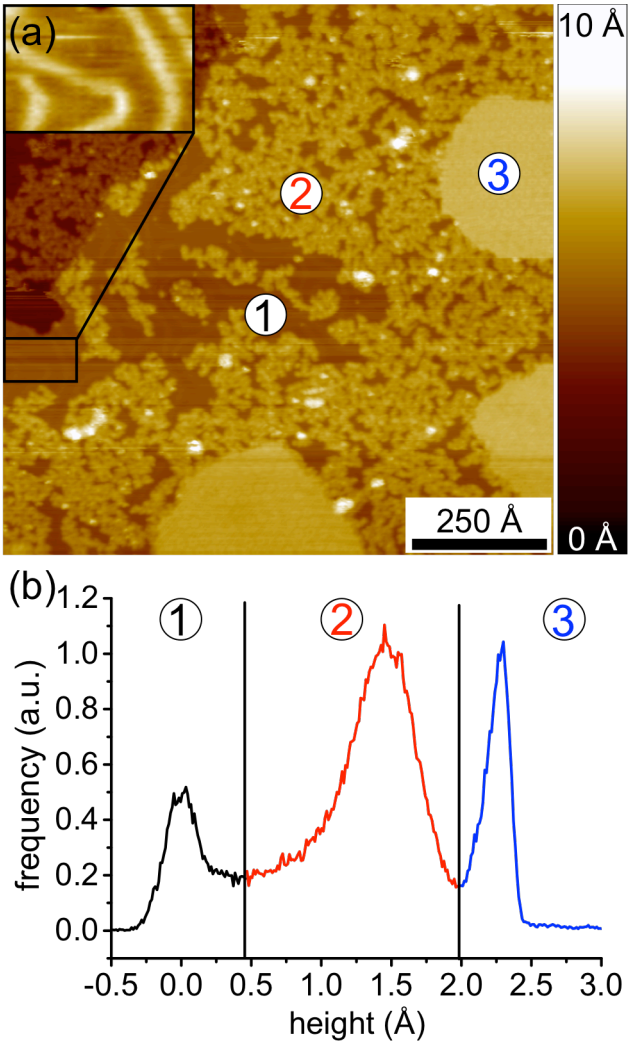

Fig. 6. Surface morphology after {Ni_4} deposition and post-annealing at 590 K. (a) STM image showing uncovered (1), disordered (2), and ordered (3) areas. The numbers are placed exemplarily on corresponding areas. Inset: A distorted herringbone reconstruction appears in uncovered areas. Image parameters: 1000 Å x 1000 Å, V_{Bias} = –2 V, I_T = 1 nA, 5 K. (b) Histogram of the height distribution on the terrace in the right half of the STM image shown in (a).

reconstruction [32,33] and very likely explain the particular case observed here. Most importantly, the observation of the herringbone reconstruction allows us to determine the particle coverage to be in the submonolayer regime and to measure the apparent height of the adsorbate layers.

The histogram of the height distribution calculated for the terrace in the right half of Fig. 6a, where no substrate step edges occur, is shown in Fig. 6b. The first peak in the histogram (black) represents the bare substrate, which takes 15% of the surface area. The average height of the substrate is set to 0 Å. The second peak (red) is attributed to the disordered areas in Fig. 6a. The disordered

nature is also confirmed by the larger width and the asymmetric shape of this peak, indicating that there is no strongly preferred height. About 65% of the surface is covered with disordered areas, and the most probable height is 1.5 Å above the Au surface. The remaining 20% of the surface exhibit ordered areas with an average relative height above the substrate of 2.2 Å. These height differences are much smaller than what we would expect for intact $\{Ni_4\}$ and are rather of the order of the corrugation of single atoms. Therefore, the STM data in Fig. 6 confirm the decomposition of the molecule. High-resolution STM images (Fig. S3 in the Supplementary Material) reveal two different adsorption symmetries in the ordered areas, pointing towards an intermediate and a final state. In order to investigate this conjecture, the samples were post-annealed in a next step to slightly higher temperatures.

3.2.3. Post-annealing at 680 K

After post-annealing at 680 K, the samples show only one hexagonal morphology (Fig. 7a). The repeating feature of this morphology is a dark central hole surrounded by six bright spots in hexagonal symmetry. The lateral distance between central holes is 9.5 Å, and the corrugation is about 0.5 Å (see Fig. S4 in the Supplementary Material for structure models of the sulfur overlayers imaged by high-resolution STM). Similar to the observations after the first annealing step, the STM images are only very weakly dependent on the bias voltage. Even for reversed bias voltage, the center hole remains a hole, indicating that the STM corrugation is mostly of topographic rather than electronic origin. LEED patterns still reveal the spots

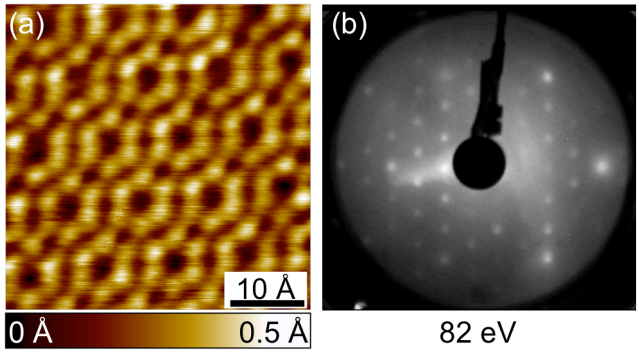

Fig. 7. High-resolution STM image and LEED pattern after $\{Ni_4\}$ deposition on Au(111) and post-annealing at 680 K for 1 hour. The LEED pattern taken at 82 eV confirms that the local structure observed in the STM image (a) coherently covers large areas on the sample surface. STM image parameters: 40 Å x 40 Å, $V_{Bias} = -1$ V, $I_T = 1$ nA, 5 K.

belonging to the Au(111)-(1x1) substrate, but in addition we observe spots forming a $2\sqrt{3}x2\sqrt{3}$ superstructure (Fig. 7b). The size and symmetry of this superstructure is in good agreement with the STM data. Therefore, the local structure observed in Fig. 7a is long-range ordered and covers large areas of the sample surface. STM data do not allow an unambiguous chemical identification of the six alike looking building blocks within the surface unit cell, but by comparison with literature data [34] and our XPS data, we can safely conclude that we observe atomic sulfur on Au.

4. Conclusions

The adsorption of a cubane-type SMM with structurally exposed thio-cyclohexane groups on the Au(111) surface has been investigated with STM, XPS and LEED techniques. We find that the organic HL·S ligands decoordinate from the $\{Ni_4Cl_{4n}\}$ core during the adsorption of the $\{Ni_4\}$ molecule, which we attribute to the released adsorption energy of S on Au. The remaining fragments very likely contribute to the disordered morphology observed by STM in the as-deposited state. Post-annealing above 480 K leads to a decomposition of the initially intact $\{Ni_4Cl_{4n}\}$ core and desorption of some fragments, while the remaining Ni- and S-containing parts form a long-range ordered superstructure at 680 K. The stability of the $\{Ni_4Cl_{4n}\}$ core up to 480 K indicates that such types of coordination complexes can be tuned to retain their SMM properties exhibited in the bulk as long as the local molecular electrostatic environment does not significantly influence the molecular magnetic anisotropy [35]. Future XMCD studies will show if charge-neutral, thioether-functionalized organic ligands can be used as transporters of highly unstable inorganic structures with appealing electronic and magnetic properties onto metallic substrates, whose interfaces are capable of providing a certain chemical stability to such elusive species (*e.g.* in our case the $\{Ni_4Cl_{4n}\}$ building block), not achievable in the bulk.

The results described herein highlight the fragility of the intramolecular, magnetic core-organic ligand interfaces, which are strongly influenced by the substrate surface upon deposition of the title coordination complex from solution. Strategies to stabilize metal-organic complexes on various metallic substrates are (i) strengthening of the metal-ligand bonds by introducing strong

π-backbonding organic ligands and/or strongly negatively charged chelating (redox) ligands and (ii) reduction of the number of ligands/anchoring groups per complex so that all of them can bind to the substrate surface with no significant molecular deformation or ligand decoordination.

Acknowledgements

We thank Sven Döring and Mathias Gehlmann for experimental support at DELTA synchrotron. K.Y.M. thanks the Excellence Initiative of the German federal and state governments for an RWTH Start-Up grant. A.G. and P.B. are grateful to the CNRS, the Ministère de la Recherche (Paris), the DFH/UFA (International Research Training Group GRK532, Ph.D. grant to A.G.), and the International Centre for Frontier Research in Chemistry, Strasbourg (icFRC, http://www.icfrc.fr).

References

[1] G. Poirier, E. Pylant, Science 272 (1996) 1145.

[2] M.H. Dishner, J.C. Hemminger, F.J. Feher, Langmuir 13 (1997) 2318.

[3] J.C. Love, L.A. Estroff, J.K. Kriebel, R.G. Nuzzo, G.M. Whitesides, Chem. Rev. 105 (2005) 1103.

[4] E. Ito, J. Noh, M. Hara, Surf. Sci. 602 (2008) 3291.

[5] M. Mannini, P. Sainctavit, R. Sessoli, C. Cartier dit Moulin, F. Pineider, M.-A. Arrio, A. Cornia, D. Gatteschi, Chem. Eur. J. 14 (2008) 7530.

[6] M. Mannini, F. Pineider, P. Sainctavit, C. Danieli, E. Otero, C. Sciancalepore, A.M. Talarico, M.-A. Arrio, A. Cornia, D. Gatteschi, Nat. Mater. 8 (2009) 194.

[7] M. Mannini, F. Pineider, C. Danieli, F. Totti, L. Sorace, P. Sainctavit, M.-A. Arrio, E. Otero, L. Joly, J. C. Cezar, Nature 468 (2010) 417.

[8] J.J. Parks, A.R. Champagne, T.A. Costi, W.W. Shum, A.N. Pasupathy, E. Neuscamman, S. Flores-Torres, P.S. Cornaglia, A.A. Aligia, C.A. Balseiro, G. K.-L. Chan, H.D. Abruña, D.C. Ralph, Science 328 (2010) 1370.

[9] J. Dreiser, A.M. Ako, C. Wäckerlin, J. Heidler, C.E. Anson, A.K. Powell, C. Piamonteze, F. Nolting, S. Rusponi, H. Brune, J. Phys. Chem. C 119 (2015) 3550.

[10] M.J. Rodriguez-Douton, M. Mannini, L. Armelao, A.-L. Barra, E. Tancini, R. Sessoli, A. Cornia, Chem. Commun. 47 (2011) 1467.

[11] A. Cornia, M. Mannini, P. Sainctavit, R. Sessoli, Chem. Soc. Rev. 40 (2011) 3076.

[12] J. Noh, T. Murase, K. Nakajima, H. Lee, M. Hara, J. Phys. Chem. B 104 (2000) 7411.

[13] E.B. Troughton, C.D. Bain, G.M. Whitesides, R.G. Nuzzo, D.L. Allara, M.D. Porter, Langmuir 4 (1988) 365.

[14] S.C. Jensen, A.E. Baber, H.L. Tierney, E.C.H. Sykes, ACS Nano 1 (2007) 423.

[15] A. Ghisolfi, K.Yu. Monakhov, R. Pattacini, P. Braunstein, X. López, C. de Graaf, M. Speldrich, J. van Leusen, H. Schilder, P. Kögerler, Dalton Trans. 43 (2014) 7847.

[16] C. Piovezan, J.M.R. Silva, A. Neves, A.J. Bortoluzzi, W. Haase, Z. Tomkowicz, E.E. Castellano, T.C.S. Hough, L.M. Rossi, Inorg. Chem. 51 (2012) 6104.

[17] A. Scheurer, A.M. Ako, R.W. Saalfrank, F.W. Heinemann, F. Hampel, K. Petukhov, K. Gieb, M. Stocker, and P. Müller, Chem. Eur. J. 16 (2010) 4784.

[18] D. Wagner, W.M. Riggs, L.E. Davis, J.F. Moulder, Handbook of X-ray Photoelectron Spectroscopy, Perkin-Elmer Corporation (Physical Electronics), 1979.

[19] M.A. van Hove, R.J. Koestner, P.C. Stair, J.P. Bibérian, L.L. Kesmodel, I. Bartos, G.A. Somorjai, Surf. Sci.103 (1981) 189.

[20] T. Weidner, N. Ballav, U. Siemeling, D. Troegel, T. Walter, R. Tacke D.G. Castner, M. Zharnikov, J. Phys. Chem. C 113 (2009) 19609.

[21] D.G. Castner, K. Hinds, D.W. Grainger, Langmuir 12 (1996) 5083.

[22] T. Ishida, N. Choi, W. Mizutani, H. Tokumoto, I. Kojima, H. Azehara, H. Hokari, U. Akiba, M. Fujihira, Langmuir 15 (1999) 6799.

[23] C.-J. Zhong, M.D. Porter, J. Am. Chem. Soc. 116 (1994) 11616.

[24] C.-J. Zhong, R.C. Brush, J. Anderegg, M.D. Porter, Langmuir 15 (1999) 518.

[25] A. Tolman, W.M. Riggs, W.J. Linn, C.M. King, R.C. Wendt, Inorg. Chem. 12 (1973) 2770.

[26] J. Matienzo, L.I. Yin, S.O. Grim, W.E. Swartz, Inorg. Chem. 12 (1973) 2762.

[27] J. Gottschalck, B. Hammer, J. Chem. Phys. 116 (2002) 784.

[28] B. Sexton, Surf. Sci. 163 (1985) 99.

[29] S. Fahrendorf, F. Matthes, D.E. Bürgler, C.M. Schneider, N. Atodiresei, V. Caciuc, S. Blügel, C. Besson, P. Kögerler, SPIN 4 (2013) 1440007.

[30] L. Zobbi, M. Mannini, M. Pacchioni, G. Chastanet, D. Bonacchi, C. Zanardi, R. Biagi, U. Del Pennino, D. Gatteschi, A. Cornia, Chem. Commun. (2005) 1640.

[31] J. Noh, M. Hara, Langmuir 18 (2002) 1953.

[32] L. Huang, P. Zeppenfeld, J. Chevrier, G. Comsa, Surf. Sci. 352 (1996) 285.

[33] F. Rossel, P. Brodard, F. Patthey, N.V. Richardson, W.-D. Schneider, Surf. Sci. 602 (2008) L115.

[34] C. Vericat, M.E. Vela, G.A. Andreasen, R.C. Salvarezza, F. Borgatti, R. Felici, T.-L. Lee, F. Renner, J. Zegenhagen, J.A. Martin-Gago, Phys. Rev. Lett. 90 (2003) 7.

[35] X. Fang, P. Kögerler, M. Speldrich, H. Schilder, M. Luban, Chem. Commun. 48 (2012) 1218.